Silicon photonic beam steering module with backside coupling elements toward dense heterogeneous integration with drive electronics

X. Chen, F. Meng, S. A. Fortune, et al.

View Online

Export Citation

CrossMark

ARTICLES YOU MAY BE INTERESTED IN

Silicon photonic beam steering module with backside coupling elements toward dense heterogeneous integration with drive electronics 🔵EP

X. Chen,[1] 🆔 F. Meng,[1] S. A. Fortune,[2] A. J. Compston,[2] M. Ebert,[1] X. Yan,[1] H. Du,[1] M. Banakar,[1] D. T. Tran,[1]
C. G. Littlejohns,[1] D. J. Thomson,[1] R. Nicolaescu,[2] and G. T. Reed[1,a]

AFFILIATIONS

[1] Optoelectronics Research Centre, Zepler Institute for Photonics and Nanoelectronics, Faculty of Engineering
and Physical Sciences, University of Southampton, Southampton SO17 1BJ, United Kingdom
[2] Pointcloud, Inc., San Francisco, California 94107, USA

[a] Author to whom correspondence should be addressed: G.Reed@soton.ac.uk

ABSTRACT

Solid state beam steering devices are key elements in low cost, robust, and three-dimensional imaging systems. Here, we present a silicon photonic beam steering device based upon an 8 × 8 grating coupler focal plane array approach fed by a thermo-optic Mach–Zehnder switching tree. In this device, transmission of light from the grating couplers is made through the backside of the chip using topside mirrors allowing for both high-efficiency out-coupling and direct flip-chip integration of drive electronics, providing a path to scale to denser focal plane arrays with large numbers of points in the future. A −13.8 dB fiber-to-fiber transmission was achieved in our preliminary test around 1523 nm for the beam steering chip.

I. INTRODUCTION

In recent years, there has been significant activity in the development of 3D imaging systems based upon LIDAR (Light Detection and Ranging) to accurately map the positions and even the velocity of objects in a 3D space.[1–6] Such systems can serve applications such as autonomous navigation, augmented reality, healthcare, and robotics. Beam steering is a key function in these systems allowing them to scan over a certain field of view with efficient use of laser power. In many commercial systems,[7–9] beam steering is performed mechanically by physically moving parts to direct and scan the beam over a certain area. While such mechanical steering has allowed the highest performances to be achieved, solid state beam steering approaches[10–14] are advantageous in terms of cost, compactness, and reliability. One proposed solid-state approach is the use of an optical phased array (OPA). However, to date, demonstrations of OPA based 2D-scanning systems have been limited to a range of ~10 m.[15–17]

Recently, we presented an alternative approach to beam steering based upon a focal plane array (FPA) consisting of 16 grating couplers, which are individually addressed using a thermo-optic Mach–Zehnder interferometer (MZI) based switching tree.[18] The light in this case is therefore routed to a single grating at a time which, in turn, illuminates a small subset of the scene using a lens system. This approach is robust, and the optical loss is only limited by waveguide scattering losses and the extinction ratio of the switching elements. Scaling to large, dense arrays of grating couplers is also achievable due to the use of frontend/monolithic integration of the electronics used to control the switching tree. While there are many advantages to frontend/monolithic integration, alternative approaches, such as heterogeneous integration, are also attractive. The heterogeneous integration of photonics and electronics

means both chips are fabricated separately and subsequently integrated using approaches such as wire bond and flip-chip bonding. This offers more flexibility, particularly in terms of optical power handling for long range imaging, and potentially a higher integration density since the photonics and control electronics reside in a different plane.

The number of electrical connections to the MZI switch tree scales linearly with the number of grating couplers, and therefore, when scaling to a large array using a wire-bond heterogeneous integration approach, the chip size can become very large, driven by the size and number of electrical pads required at the edges of the chip. Flip-chip bonding or similar 3D integration schemes,[19,20] on the other hand, can provide integration to a dense array of electrical pads across the top surface of the chip. The challenge then is that integration on the topside of the photonic chip can inhibit the transmission of the light from the grating couplers, particularly in this application area. Therefore, high-efficiency grating designs for backside coupling are required.[21,22] In this paper, we present a proof-of-concept demonstration of an FPA based beam steering module comprising an array of 8 by 8 grating couplers. A metal mirror layer was deposited on the topside of the grating couplers to enhance transmission of the light to the backside of the chip.[23,24] With the light exiting the chip from the backside, the topside is free for electrical connection to control the switches which, in this case, has been performed by first flip-chip bonding onto a printed circuit board (PCB) and then ultimately connected to electronic control boards. Further developments in this work can involve the integration of a custom electronic drive chip to be directly bonded on top of the photonic chip. The photonic beam steering chip has been formed using silicon photonic technology. The maturity of silicon photonic technology driven by years of intense development for data communication applications allows for the dense integration of photonic elements with high reliability and low-cost manufacturing, which is highly attractive for this application.

This work demonstrates the capability to realize a beam steering module using our backside emission and heterogeneous integration approach. It can open up a range of manufacturing options and provide a path toward highly dense arrays of grating couplers. An additional benefit of using mirrors to direct all of the light to the backside of the chip is that the transmission efficiency is not limited by the directionality of the grating coupler. By optimizing the design parameters and assuming a perfect anti-reflection (AR) coating at the backside of the wafer, we can theoretically achieve 95% directionality to the backside of a wafer and 84% coupling efficiency to the fiber mode, which is about a 2 dB improvement in coupling efficiency compared to topside coupling gratings fabricated on the same platform.

II. PHOTONIC CHIP DESIGN

The photonic chip was designed for the 220 nm silicon on 2000 nm buried oxide waveguide platform. Rib waveguides with 100 nm slab height were used to minimize propagation losses. The circuit consists of two main elements: backside grating couplers for feeding light into the circuit and coupling out into free space and a switching tree for routing the light to the individual out-couplers.

A. Input and output coupling

Coupling of light into and out of the circuit is performed using grating couplers. Metallic mirrors are positioned above them on the topside to ensure a high coupling efficiency through the backside of the chip. As shown in Fig. 1(a), the gratings were formed with a 60 nm shallow-etch into the top silicon waveguide layer. 2D FDTD (two-dimensional finite-difference time-domain) simulations were used to simulate the grating diffraction. The grating couplers were designed for coupling the TE (transverse electric) mode with a center wavelength of 1550 nm. The boundary conditions were set to a PML (perfectly matched layer).

Fibers were aligned to the surface of the SOI wafer with a tilting angle of $\theta = 10°$ off normal, which means that the diffracted light beam from the grating is 6.8° off normal in the oxide cladding and 10° off normal in air. The period of the grating coupler is 610 nm, with a fill factor of 0.5 (defined as the ratio of etched slit width over the grating period Λ). The metal mirror (200 nm thick) made of aluminum was deposited on top to reflect the light downward to the backside of the chip as shown in Fig. 1(a). According to our calculation, over 95% of light was coupled downward with the metal mirror on top. The oxide thickness between the metal mirror and the top of the silicon surface is 830 nm, which was optimized to maximize the coupling efficiency. Standard uniform gratings as illustrated in Fig. 1(b) were used in this case as the input coupling from fiber to the beam steering chip. The calculated coupling efficiency to the single-mode fiber with a mode field diameter of 10.4 μm is 84% (−0.76 dB) around 1550 nm wavelength. The field profile calculated by the 2D FDTD simulation for the uniform gratings is shown in Fig. 2(a). We also assume that the lateral modal profile of the waveguide (y axis) is matched with the single-mode fiber,[25] and there is no additional loss at the bottom surface of the wafer (with a perfect AR coating layer).

Uniform focusing grating couplers as shown in Fig. 1(c) were used for out-coupling to free space. The focusing grating couplers used as output in our demonstrated beam steering chip are not standard focusing grating couplers optimized for coupling to fibers. They are smaller in order to be densely packed into a two-dimensional array. The near field and far field profiles of the light coupled out
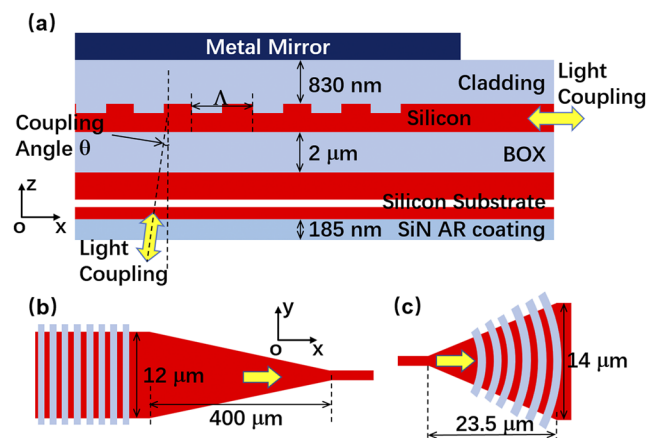

FIG. 1. Schematic illustrations of the backside grating couplers: (a) side view, (b) top view of the uniform grating couplers as the input, and (c) top view of the focusing grating couplers for the output of the beam steering module.
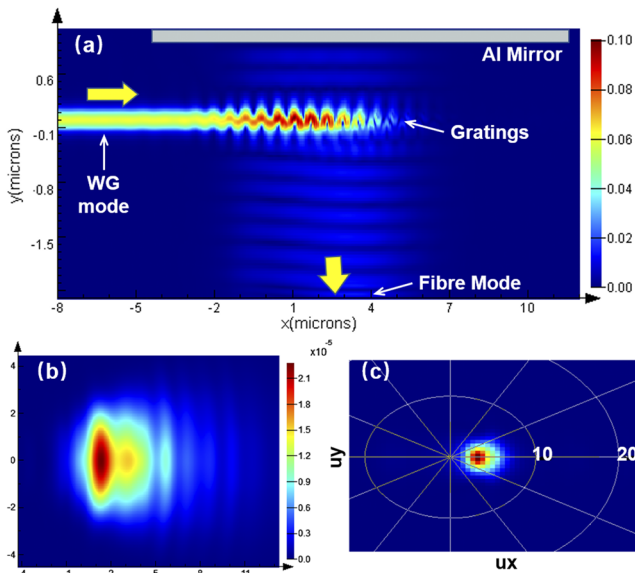
FIG. 2. (a) Field profile of the 2D FDTD simulation while coupling between the fiber and the waveguide. (b) Near field profile of the light from the output grating (in silicon substrate, 2.2 μm below the grating). (c) Far field profile of the light from the output grating calculated in silicon substrate [same as (b)].

from this output grating are shown in Figs. 2(b) and 2(c). The light from the output grating can be collected by a set of collimating lenses and projected to the objects in the distant scene. Following emission from the chip, the light can be collimated by a set of lenses to illuminate the scene being imaged. As we are using a focal plane array (FPA) approach instead of an optical phase array (OPA), the projected beam spot size and field of view (FOV) will both depend on the parameters of the projection lens system, which can be fine-tuned according to the required LIDAR resolution.

B. Switching tree

The switching tree is used to selectively route the input light to one of the 64 output couplers in the FPA. The switching tree in this case uses six stages of 1 × 2 thermo-optic MZI optical switches. A diagram showing a single unit switch is shown in Fig. 3.

2 × 2 multi-mode Interferometer (MMI) were used to split and recombine the light to and from the MZI arms. On top of one waveguide arm, a TiN heating element is positioned to control its
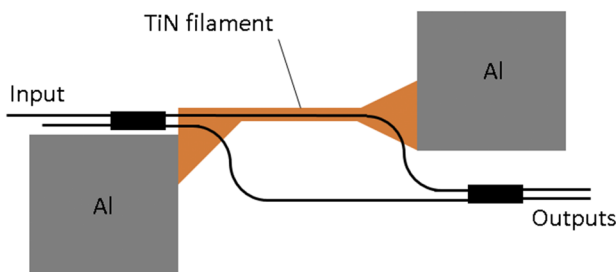

FIG. 3. Diagram of a single thermo-optic MZI based optical switch.

temperature electrically. The titanium nitride filament had dimensions of length 120 mm, width 2 mm, and thickness 400 nm. These values were specifically chosen to optimize the power efficiency of the switching process and provide a resistance of ~550 Ω to be compatible with the driving electronics. After the sixth stage in the switching tree, the 64 output waveguides were each routed to one of the output grating couplers.

III. FABRICATION

The fabrication flow is depicted in Fig. 4. First, photoresist was spin coated onto the topside of the wafers and HF etching was used to strip the silicon dioxide layer on the backside. Next, a 1 μm thick silicon dioxide layer was deposited on the topside of the wafer by plasma enhanced chemical vapor deposition (PECVD), which provided protection to the silicon layer on the topside during chemical mechanical polishing (CMP) of the backside. The CMP step was performed to make the backside optically smooth for efficient backside emission. Because metal-contaminated wafers are not allowed in the CMP machine in our facility, the CMP step was performed at the beginning of the process, and it could equally be performed at the end of the process. A 185 nm thick layer of silicon nitride was then deposited on both sides of the wafer by low pressure chemical vapor deposition (LPCVD) to give protection to the backside and to act as an anti-reflection layer to light exiting from the backside of the chip. The roughness of the backside surface of the wafer was 0.28 nm, measured by AFM.

The silicon nitride and silicon dioxide layers were then stripped from the frontside of the chip by dry and chemical etching. Following this, 248 nm deep ultraviolet (DUV) lithography was used to expose the grating couplers in photoresist before inductively coupled plasma (ICP) etching of 60 nm into the topside silicon overlayer. Two further DUV lithography and ICP etching steps were
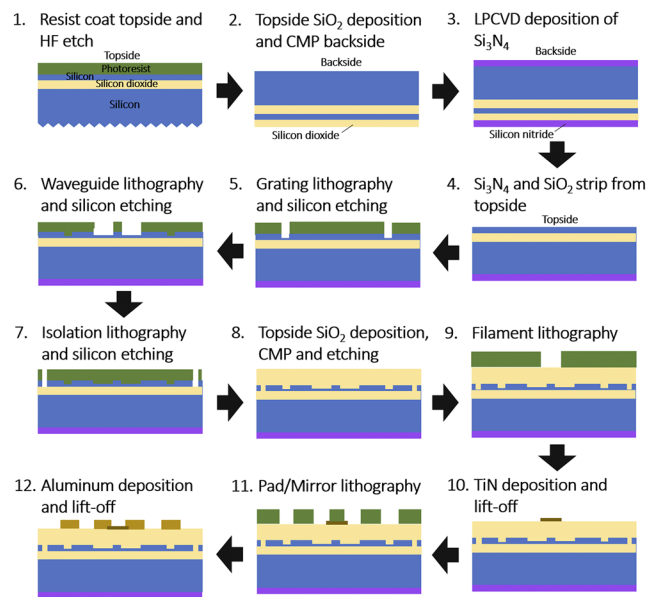

FIG. 4. Fabrication flow of the silicon photonic focal plane array beam steering chip.
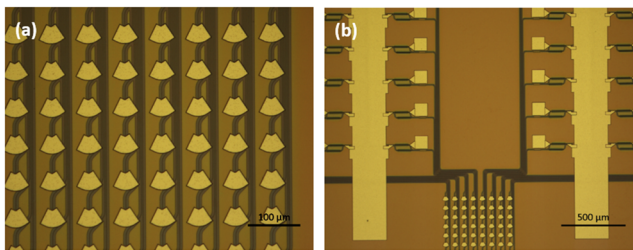
FIG. 5. Microscope images of the fabricated device: (a) grating array and (b) the switching tree with MZIs.

FIG. 6. Photograph of the silicon photonic beam steering chip mounted on the printed circuit board: (a) top view and (b) side view.

used to define the waveguides (120 nm etch depth) and isolation trenches (220 nm etch depth). A 1 μm thick silicon dioxide cladding layer was then deposited on the topside of the wafer, CMP was used to planarize the top surface, and then silicon dioxide etching was used to thin it to the required thickness (830 nm). Next, two DUV lithography, metal deposition, and lift-off steps were used to define first the titanium nitride heater filaments and then aluminum pads for electrical connection to the filament and to act as the mirrors above the grating couplers. The optical microscope images of the chip showing the grating coupler array with aluminum mirrors and a broader view of the chip showing part of the switching tree and the waveguide connections to the grating array can be seen in Fig. 5.

IV. INTEGRATION AND ELECTRONIC DRIVING

After dicing and cleaning, the silicon photonic beam steering chip electrical connection to the control electronics was performed by flip-chip bonding to a custom designed printed circuit board (PCB). First, gold bumps were placed on the pads of the photonic chip. Next, the chip was aligned and flip-chip bonded to the PCB using a FineTech flip chip bonder. Due to the limitations on the size of PCB that could be positioned in the flip-chip bonder, this first PCB measured just 27 × 30 mm^2. This PCB was then mounted on a second, larger PCB via a standard electrical pin connector. The larger second PCB allowed for robust mounting in the optical test setup and for a ribbon electrical wire connection carrying different electrical signals, which are passed to each of the individual thermo-optic MZI switches. Photographs of the chip mounted on the two PCBs are shown in Fig. 6.

The electrical signals to supply each of the switches were produced on a third PCB interfaced with a control field programmable gate array (FPGA). A block diagram of circuit on the third PCB is shown in Fig. 7. Since light transmission is required from just one grating at a time, only one MZI in each stage of the switching tree needs to be driven for each output state. Each stage of the switching tree, therefore, requires only one digital to analog converter (DAC) and buffer to set the required voltage. An 8-bit DAC and a 5 V voltage supply were chosen to provide sufficient granularity in the voltage levels (0.02 V per level) to ensure that the MZI switches could be accurately tuned to provide a large extinction ratio and low optical loss. For an 8 by 8 array having 64 different outputs, a six-stage switching tree is required. Beyond the first stage, which contains just a single MZI switch, a demultiplexer (DEMUX) is used to switch the electrical signal to the required optical switch in each
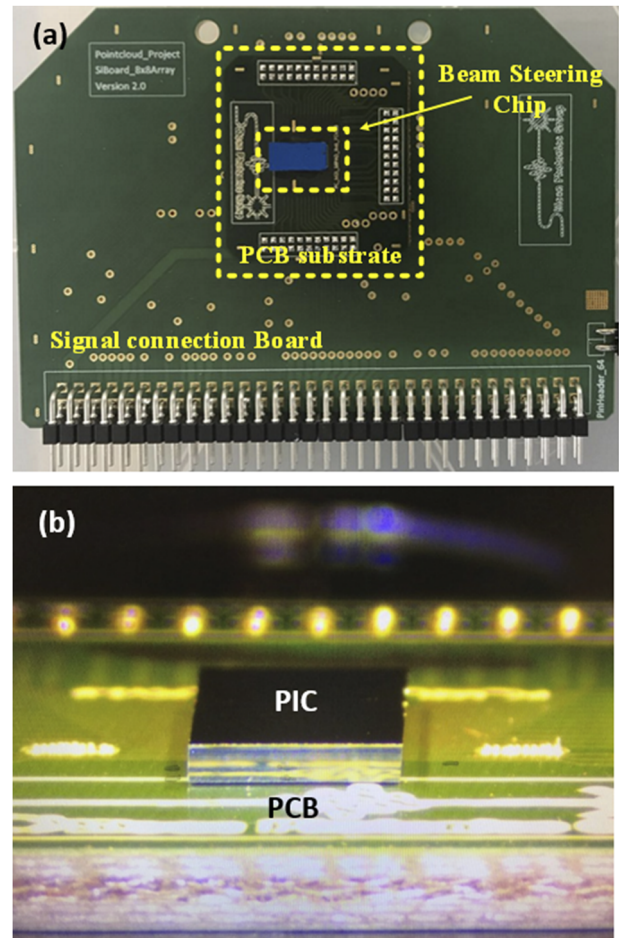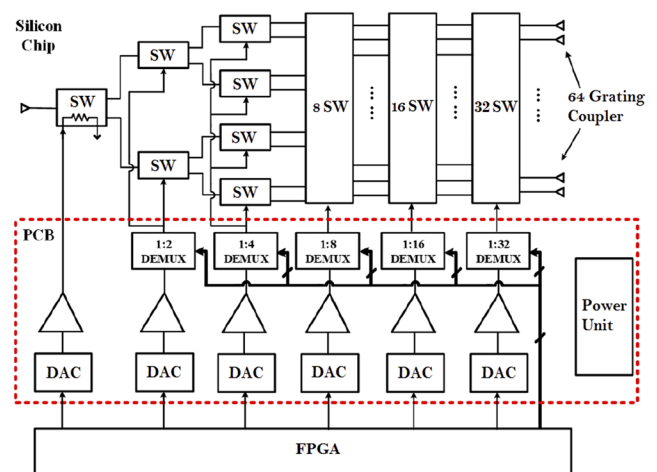

FIG. 7. Electronic circuit used to drive the beam steering element so that light output can be switched among the output gratings in an 8 × 8 array.

stage of the tree. For this proof-of-concept demonstration, the entire electrical circuit was realized with discrete, commercially available components. Such a circuit could equally be realized within a custom designed electronic integrated circuit. Control of the six DACs and five DEMUX chips was performed using an FPGA (Altera IV).

V. RESULTS AND DISCUSSION

In order to couple light into and out of the circuit through the backside of the chip, fiber focusers with pigtailed single-mode fibers were used (12.4 mm working distance). These avoided the beam divergence that would have been experienced with regular fibers. Initial alignment was performed by imaging through the chip using a near infrared camera. Upon detection of first light, alignment was optimized by measuring the transmission level on a photodetector while finely adjusting the relative positions of the fiber focusers. Due to phase errors, which are typical in submicron silicon photonic waveguides, the voltage required for the two switching states of each MZI in the circuit differed across the chip, and they needed to be accurately determined. A calibration process was therefore first performed to optimize the voltage levels at each stage for maximum transmission from each output grating sequentially. Once calibrated, test programs were run to demonstrate example scan patterns that can be produced. Measurements of the transmission through the photonic circuit were then also possible.

A typical transmission spectrum for the output ports of the beam steering module chip is shown in Fig. 8. The total fiber-to-fiber transmission was measured to be −13.8 dB at around 1523 nm. This was measured by maximizing the transmission of the output power of one output grating in the 8 by 8 array. The optical power was launched at the input grating coupler using a single-mode fiber focuser. The predicted spot size will be around 10.5 μm at a working distance of 12.4 mm. The output power was collected by the same type of fiber focuser pigtailed with a single-mode fiber, as used for the input coupling. However, the output gratings of the beam steering module are designed to couple to free space with a lens system for real applications. The actual transmission of the chip will be slightly higher, eliminating the mode mismatch with the single-mode fiber.
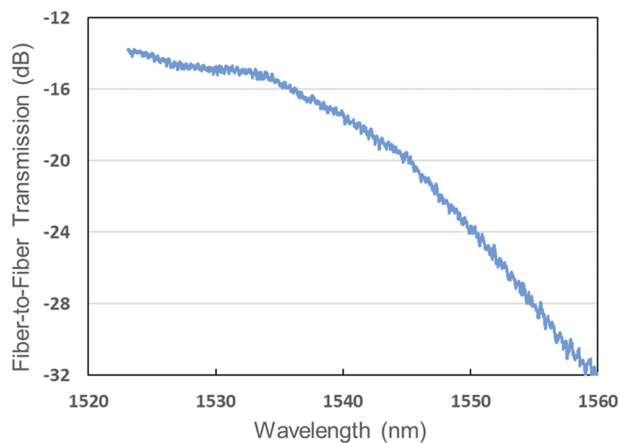
We found that the peak wavelength of the grating couplers was blue shifted from the original design. This is mainly due to the top silicon thickness of the SOI wafer used, which is only 210 nm according to our measurement as opposed to the target thickness of 220 nm [see Fig. 9(b)]. Aside from the photonic circuit of the beam steering module, several test structures were fabricated to enable characterization of the performance of the different elements within it. The coupling efficiency of the standard input grating couplers as illustrated in Fig. 1(b) was measured to be −1.8 dB (66%), as shown in Fig. 9(a). The peak wavelength was blue shifted to around 1525 nm due to the same silicon thickness issue mentioned previously. The coupling efficiency of the output grating couplers as illustrated in Fig. 1(c) was measured to be around −3.3 dB (46.8%), coupling to single-mode fibers using fiber focusers. As mentioned previously in Sec. II A, the output gratings are designed with a much smaller size than the input gratings; therefore, the output mode profile is not matched with single-mode fibers. Simulation shows that the coupling efficiency is only 58% (−2.4 dB) when coupling to a single-mode fiber. The actual coupling efficiency of the output gratings should be higher when collecting light using the lens system as designed. The waveguide (450 nm width) loss was measured via the cut-back method across various chips, and we found that the propagation loss varies between 3 and 6 dB/cm.

The highest power allowed in this photonic chip is limited by two-photon absorption (TPA).[25] According to our measurement, the maximum optical power possible in the input waveguide is around 50 mW without suffering an obvious TPA loss. To improve power handling, the waveguides can be made wider in straight sections to reduce the optical power density. Using a reverse-biased PIN diode fabricated around the waveguide to sweep out free carriers[26] can also help further improve power handling. Finally, one major advantage of our integration approach is that it allows flexibility over the waveguide platform, and therefore, a higher power handling version can be implemented by using a thicker silicon guiding layer.

The normalized transmission through a single thermo-optic MZI switch against electrical power applied to the heating element in one of the MZI arms is shown in Fig. 10. The peak normalized transmission is measured to be −0.4 dB, and the electrical power required to switch between its two states (π phase shift) is 19.5 mW. The test structures used to extract the loss of the 2 × 2 MMI used in the MZI switch indicated a loss of 0.1 dB.

FIG. 8. A typical measured transmission spectrum of the beam steering module.
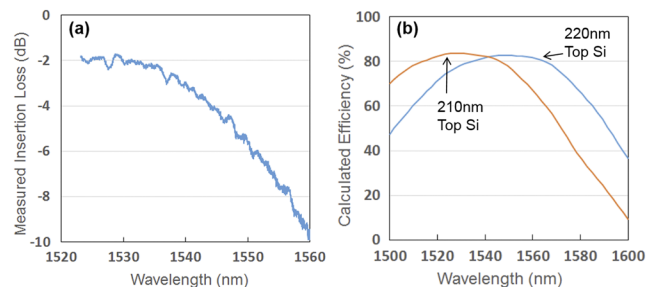

FIG. 9. (a) Coupling efficiency of the standard input grating couplers. (b) Simulated coupling efficiency for the grating couplers with 220 and 210 nm top silicon thickness.
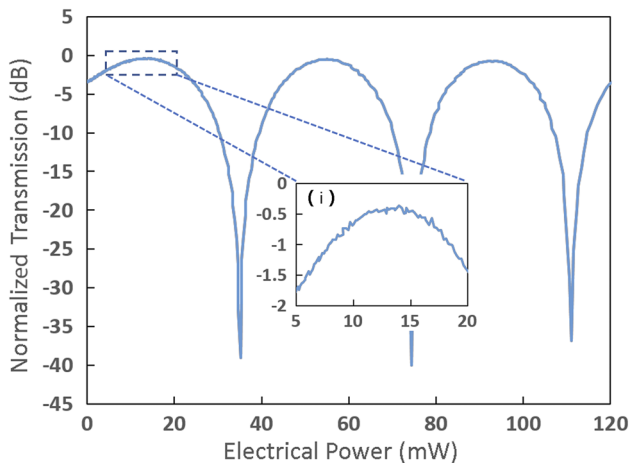
FIG. 10. Normalized transmission through the test MZI against electrical power applied to the heating element in one arm. A magnified area of the peak transmission is shown in the inset.

TABLE I. Estimated insertion loss for each component of the beam steering chip.

Components	Estimated loss (dB)
Grating input	1.8
MZI × 6	2.4
Bending loss	0.6
Grating output	3.3
Waveguide loss	5.7

As mentioned before, the overall insertion loss of the 8 by 8 beam steering chip is measured to be 13.8 dB around 1523 nm. The insertion loss for each component on the chip is listed in Table I.

Those losses are higher than our expectation, mainly due to the imperfections in the fabrication process. By improving the fabrication process, our proposed beam steering chip should have a much lower insertion loss. According to our previous experience, we would expect <1 dB coupling efficiency for the grating couplers, 0.25 dB insertion loss for each MZI, and about 2.3 dB/cm propagation loss for the waveguides.

In this proof-of-concept demonstration, the large optical path length results from limitations on the minimum pad and via the size offered by the PCB vendor, which necessitated the MZI switching elements to be spread relatively far apart on the photonic chip. By using a higher specification PCB or directly flip-bonding a control electronic integrated circuit, the packing density of the photonics could be improved dramatically. This would lead to a major reduction of the total optical path length and therefore propagation loss. Similarly, process optimization and refinements in the photonic element designs can yield further loss reductions.

VI. CONCLUSION

We have demonstrated a silicon photonic beam steering device based upon an 8 by 8 grating coupler focal plane array approach fed by a thermo-optic Mach–Zehnder switching tree. A backside coupling scheme was employed for this device using grating couplers with metal mirrors on the top. This approach allows for both high-efficiency out-coupling and high-density flip-chip integration of drive electronics providing a path to scale to a much denser focal plane array containing a large number of points in the future. The overall insertion loss of the beam steering chip was measured to be 13.8 dB. A coupling efficiency of 66% (−1.8 dB) was measured for the uniform grating couplers. Further improvement can be realized by fine-tuning the fabrication process and applying an apodizing grating design to the grating couplers.[27] This work demonstrates the capability to realize a beam steering module using a heterogeneous integration approach opening up a range of manufacturing options and photonic platforms as well as providing a path toward highly dense arrays.

SUPPLEMENTARY MATERIAL

See the supplementary material for a video showing the scanning operation of the beam steering module.

AUTHOR DECLARATIONS

Conflict of Interest

The project was funded by Pointcloud, Inc., a start-up company that makes laser ranging devices based on coherent receiver arrays. S.A.F., A.J.C., D.J.T., R.N., and G.T.R. are shareholders of Pointcloud, Inc.

DATA AVAILABILITY

The data that support the findings of this study are openly available in the University of Southampton Institutional Research repository at http://doi.org/ePrints.soton.ac.uk.[28]

REFERENCES

[1] C. Urmson, J. Anhalt, D. Bagnell et al., "Autonomous driving in urban environments: Boss and the Urban challenge," J. Field Rob. **25**(8), 425–466 (2008).
[2] J. Wang, W. Sun, W. Shou, X. Wang, C. Wu, H.-Y. Chong, Y. Liu, and C. Sun, "Integrating BIM and LiDAR for real-time construction quality control," J. Intell. Rob. Syst. **79**, 417–432 (2015).
[3] J. Hecht, "LIDAR for self-driving cars," Opt. Photonics News **29**(1), 26–33 (2018).
[4] B. Behroozpour, P. A. M. Sandborn, M. C. Wu, and B. E. Boser, "Lidar system architectures and circuits," IEEE Commun. Mag. **55**(10), 135–142 (2017).
[5] A. Kasturi, V. Milanovic, B. H. Atwood, and J. Yang, "UAV-borne lidar with MEMS mirror-based scanning capability," Proc. SPIE **9832**, 98320M (2016).
[6] Q. Wang and M.-K. Kim, "Applications of 3D point cloud data in the construction industry: A fifteen-year review from 2004 to 2018," Adv. Eng. Inf. **39**, 306–319 (2019).
[7] R. Halterman and M. Bruch, "Velodyne HDL-64E lidar for unmanned surface vehicle obstacle detection," Proc. SPIE **7692**, 76920D (2010).

[8]H. W. Yoo, N. Druml, D. Brunner, C. Schwarzl, T. Thurner, M. Hennecke, and G. Schitter, "MEMS-based lidar for autonomous driving," Elektrotech. Informationstech. **135**, 408–415 (2018).

[9]D. Wang, C. Watkins, and H. Xie, "MEMS mirrors for LiDAR: A review," Micromachines **11**(5), 456 (2020).

[10]F. Aflatouni, B. Abiri, A. Rekhi, and A. Hajimiri, "Nanophotonic coherent imager," Opt. Express **23**(4), 5117–5125 (2015).

[11]A. Martin et al., "Photonic integrated circuit-based FMCW coherent LiDAR," J. Lightwave Technol. **36**(19), 4640–4645 (2018).

[12]D. Inoue, T. Ichikawa, A. Kawasaki, and T. Yamashita, "Demonstration of a new optical scanner using silicon photonics integrated circuit," Opt. Express **27**(3), 2499–2508 (2019).

[13]C. Li, X. Cao, K. Wu, X. Li, and J. Chen, "Lens-based integrated 2D beam-steering device with defocusing approach and broadband pulse operation for Lidar application," Opt. Express **27**(23), 32970–32983 (2019).

[14]K. Hu, Y. Zhao, M. Ye, J. Gao, G. Zhao, and G. Zhou, "Design of a CMOS ROIC for InGaAs self-mixing detectors used in FM/cw LADAR," IEEE Sens. J. **17**(17), 5547–5557 (2017).

[15]C. V. Poulton, A. Yaacobi, D. B. Cole, M. J. Byrd, M. Raval, D. Vermeulen, and M. R. Watts, "Coherent solid-state LIDAR with silicon photonic optical phased arrays," Opt. Lett. **42**(20), 4091–4094 (2017).

[16]S. A. Miller, C. T. Phare, Y. Chang, X. Ji, O. A. Jimenez Gordillo, A. Mohanty, S. P. Roberts, M. C. Shin, B. Stern, M. Zadka, and M. Lipson, "512-element actively steered silicon phased array for low-power LIDAR," in Conference on Lasers and Electro-Optics, San Jose, CA, 2018, paper JTh5C.2.

[17]C. V. Poulton, M. J. Byrd, P. Russo, E. Timurdogan, M. Khandaker, D. Vermeulen, and M. R. Watts, "Long-range LiDAR and free-space data communication with high-performance optical phased arrays," IEEE J. Sel. Top. Quantum Electron. **25**(5), 1–8 (2019).

[18]C. Rogers, A. Y. Piggott, D. J. Thomson, R. F. Wiser, I. E. Opris, S. A. Fortune, A. J. Compston, A. Gondarenko, F. Meng, X. Chen, G. T. Reed, and R. Nicolaescu,

"A universal 3D imaging sensor on a silicon photonics platform," Nature **590**, 256–261 (2021).

[19]J. H. Lau, "Recent advances and new trends in flip chip technology," J. Electron. Packag. **138**(3), 030802 (2016).

[20]M.-J. Lee, A. R. Ximenes, P. Padmanabhan, T.-J. Wang, K.-C. Huang, Y. Yamashita, D.-N. Yaung, and E. Charbon, "High-performance back-illuminated three-dimensional stacked single-photon avalanche diode implemented in 45-nm CMOS technology," IEEE J. Sel. Top. Quantum Electron. **24**(6), 1–9 (2018).

[21]N. Mangal, B. Snyder, J. Van Campenhout, G. Van Steenberge, and J. Missinne, "Monolithic integration of microlenses on the backside of a silicon photonics chip for expanded beam coupling," Opt. Express **29**(5), 7601 (2021).

[22]D. Fowler, Q. Wilmart, S. Garcia, S. Olivier, and B. Szelag, "Fiber grating couplers for optical access via the chip backside," J. Lightwave Technol. **39**(2), 557 (2020).

[23]C. Kopp, E. Augendre, R. Orobtchouk, O. Lemonnier, and J.-M. Fedeli, "Enhanced fiber grating coupler integrated by wafer-to-wafer bonding," J. Lightwave Technol. **29**(12), 1847–1851 (2011).

[24]B. Chen, X. Zhang, J. Hu, Y. Zhu, X. Cai, P. Chen, and L. Liu, "Two-dimensional grating coupler on silicon with a high coupling efficiency and a low polarization-dependent loss," Opt. Express **28**(3), 4001–4009 (2020).

[25]H. K. Tsang, C. S. Wong, and T. K. Liang, "Optical dispersion, two-photon absorption and self-phase modulation in silicon waveguides at 1.5 μm wavelength," Appl. Phys. Lett. **80**, 416 (2002).

[26]H. Rong, A. Liu, R. Jones et al., "An all-silicon Raman laser," Nature **433**, 292–294 (2005).

[27]X. Chen, C. Li, C. K. Y. Fung, S. M. G. Lo, and H. K. Tsang, "Apodized waveguide grating couplers for efficient coupling to optical fibers," IEEE Photonics Technol. Lett. **22**(15), 1156–1158 (2010).

[28]Dataset to be published on the University of Southampton Institutional Research Repository, ePrints.soton.ac.uk.